Table S1. Residual velocity (speed and direction) of the daily averaged ADCP data, percentage good (non-flagged) daily average values, major and minor semi-axes of the M2 tidal current ellipse.

			Daily averaged			M2 tidal ellipse	
Bin	Hgth (m)	Depth (m)	Speed (cm/s)	Dir (°)	Good (%)	Major (cm/s)	Minor (cm/s)
1	17	385	4.9	208	100.0	16.5	6.4
2	27	375	4.2	212	100.0	18.0	4.8
3	37	365	3.0	216	100.0	19.7	2.7
4	47	355	1.6	215	100.0	21.4	0.6
5	57	345	0.6	140	100.0	23.1	1.4
6	67	335	1.9	83	100.0	24.6	3.1
7	77	325	3.4	77	100.0	26.0	4.7
8	87	315	4.9	76	100.0	27.3	6.1
9	97	305	6.2	74	100.0	28.6	7.5
10	107	295	7.4	73	100.0	29.7	8.6
11	117	285	8.6	71	100.0	30.7	9.4
12	127	275	9.7	70	100.0	31.5	10.2
13	137	265	10.8	70	100.0	32.2	11.0
14	147	255	11.9	70	100.0	33.1	11.6
15	157	245	13.0	71	100.0	34.0	12.4
16	167	235	14.0	71	100.0	34.9	13.1
17	177	225	14.9	71	100.0	35.9	13.7
18	187	215	15.8	72	100.0	36.7	14.4
19	197	205	16.7	72	100.0	37.4	14.9
20	207	195	17.5	72	100.0	37.8	15.3
21	217	185	18.4	73	100.0	38.2	15.6
22	227	175	19.2	73	100.0	38.4	15.9
23	237	165	20.0	73	100.0	38.8	16.3
24	247	155	20.9	73	100.0	39.3	16.5
25	257	145	21.6	72	100.0	39.6	16.7
26	267	135	22.1	73	100.0	39.7	16.9
27	277	125	22.6	73	99.6	40.3	17.0
28	287	115	22.4	74	96.8	40.7	16.8
29	297	105	21.8	75	92.1	41.8	16.6
30	307	95	20.9	77	86.3	41.5	16.4

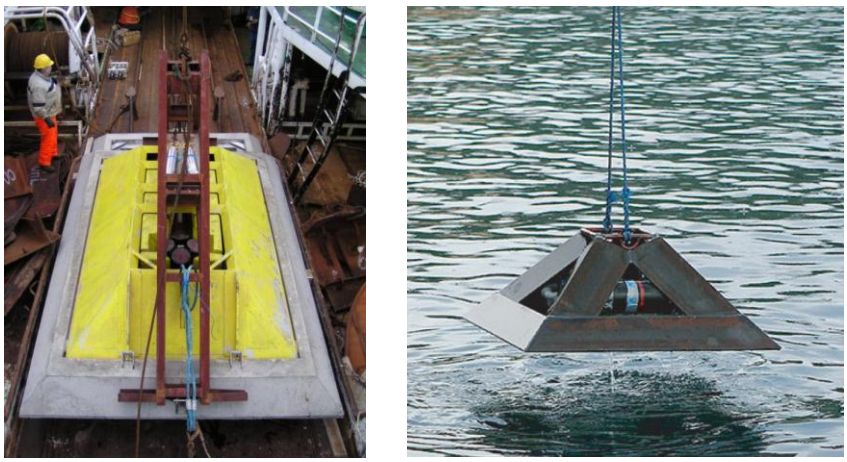

Figure S1. Left panel: An ADCP in a trawl-proof frame (yellow) onboard a research vessel, ready for deployment. Right panel: A bottom temperature logger (BTL) including temperature sensor, acoustic modem, and batteries in a trawl-proof frame.

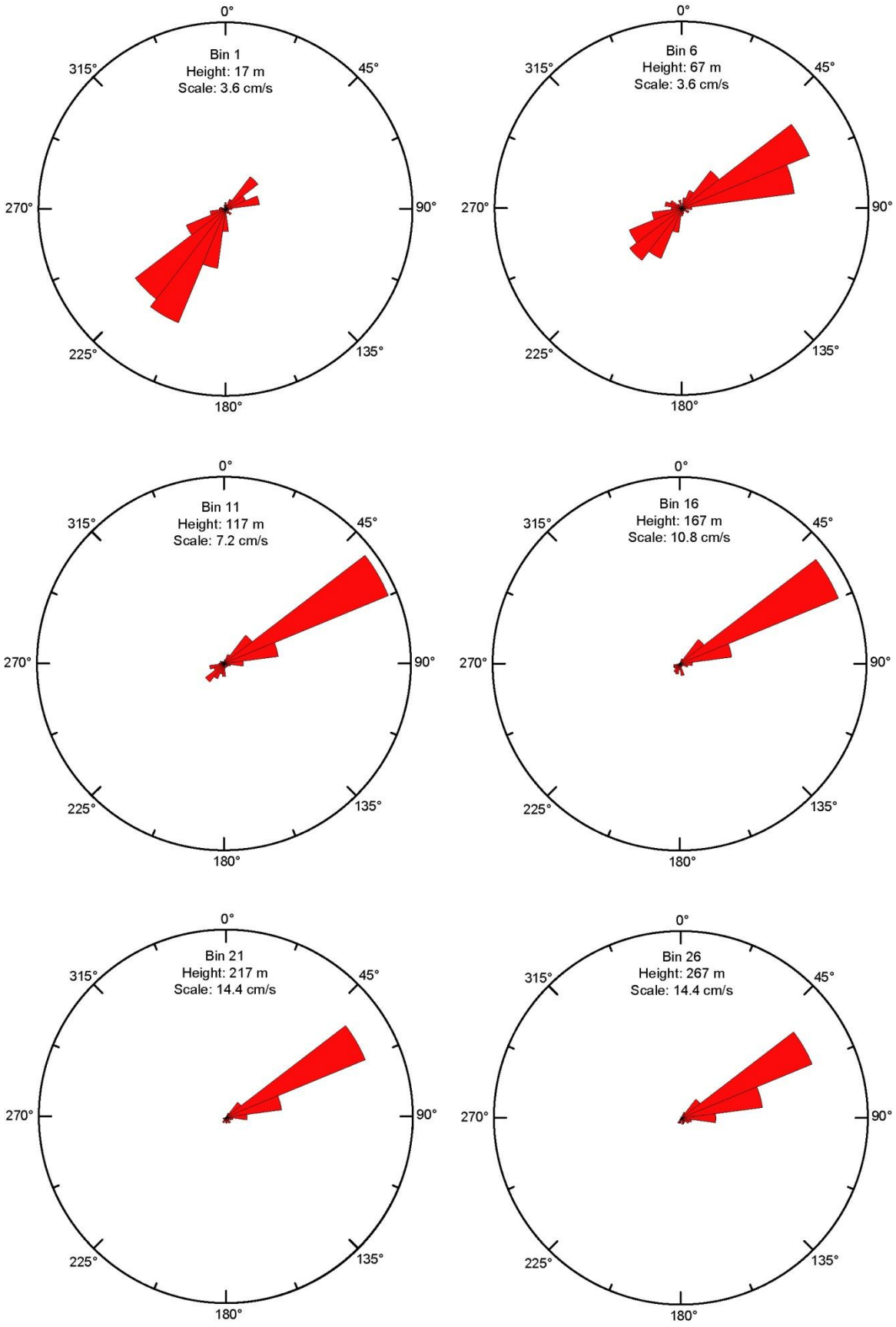

Figure S2. Average velocity in 15° directional classes for six bins from the ADCP data at site B. The average velocity is represented by the "height" of each triangular section with the radius of the circle representing the velocity indicated by "Scale".

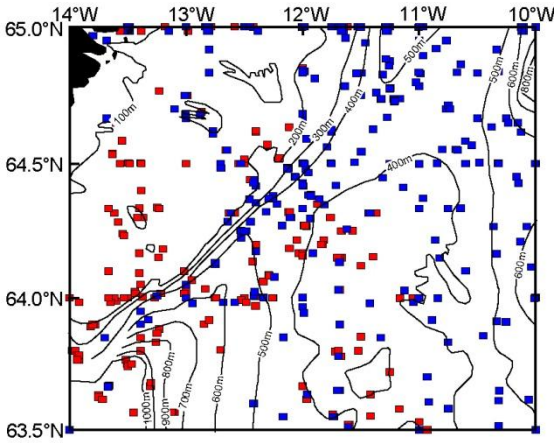

Figure S3. Bottom temperatures above (red squares) and below (blue squares) 3 °C from historical CTD profiles. Only profiles with the CTD reaching less than 40 m from bottom are included.

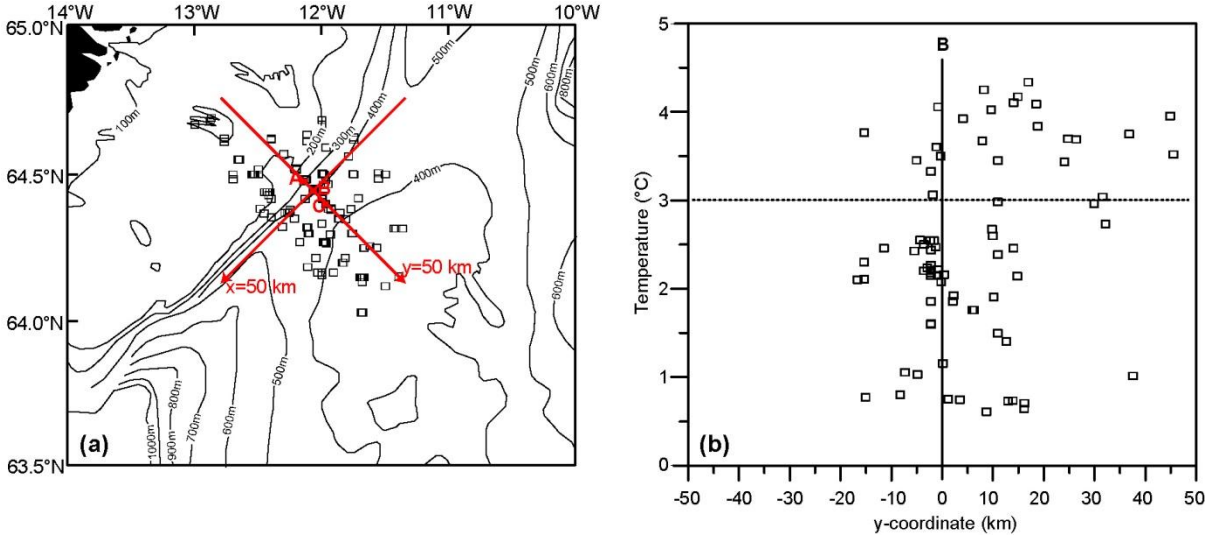

Figure S4. (a) Selected CTD stations in the sill region with coordinate system indicated by red arrows. **(b)** Variation along the y-axis of the temperature for which σ_θ = 27.8 kg m^{-3}. The vertical line at y = 0 indicates site B. The hatched horizontal line indicates 3 °C.

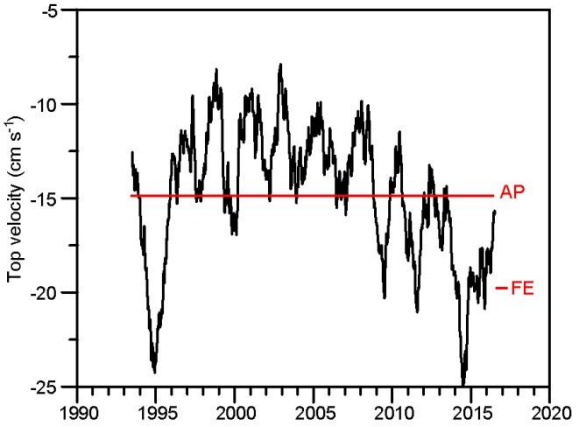

Figure S5. Annually averaged (365-day running mean) top velocity from 1993 to 2016 based on satellite altimetry and the established regression equation (Sect. 3.2 in the main manuscript). Red lines indicate the estimated top velocity averaged over the duration of the field experiment (FE) and over the altimetry period from 1993 to 2016 (AP).

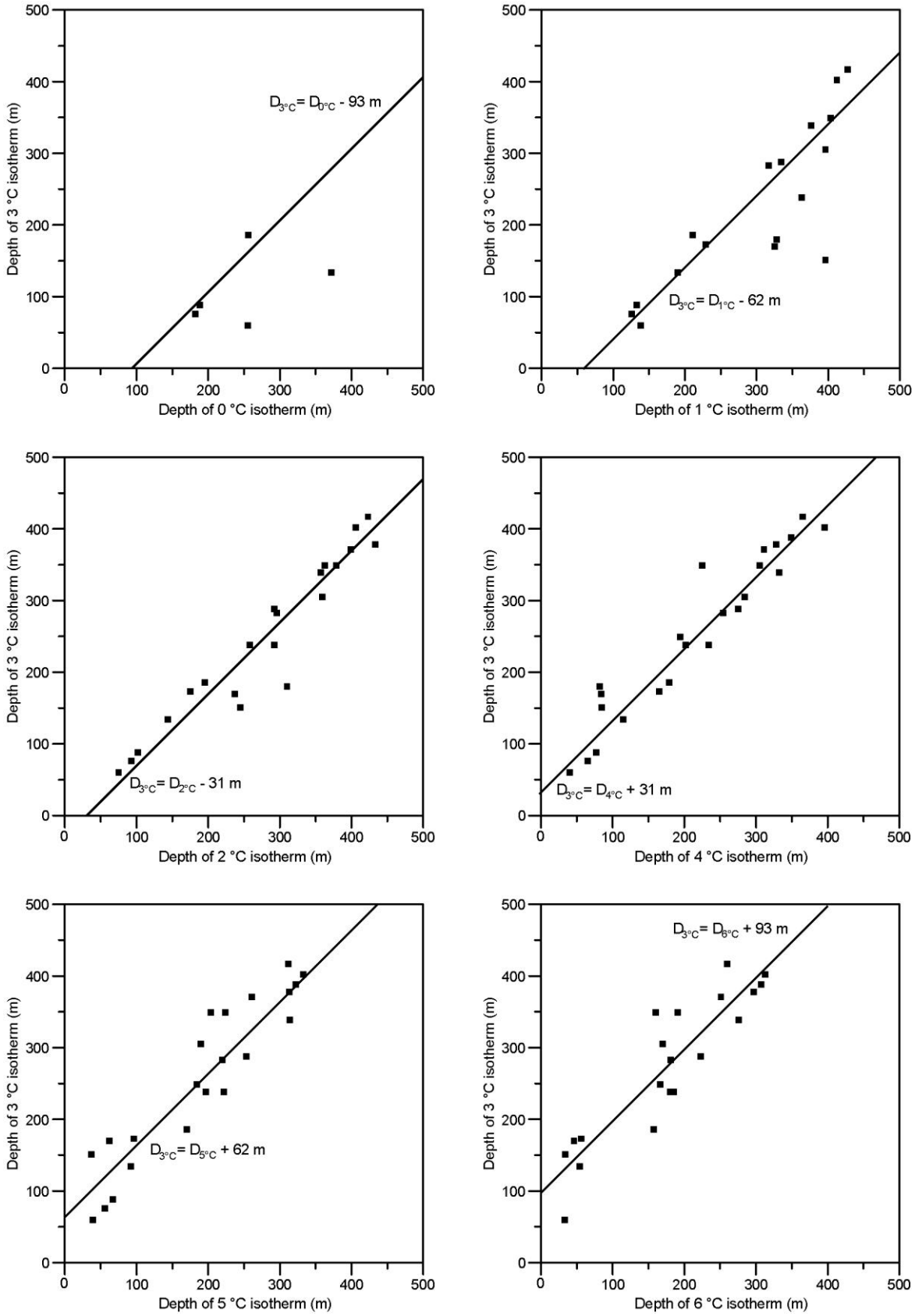

Figure S6. Depth of the 3 °C isotherm, $D_{3°C}$, plotted against depths of other isotherms as determined from the CTD stations deeper than 300 m on Fig. 9a in the main manuscript. The lines represent the relationships assuming that vertical distances between isotherms are constant and equal to the temperature difference multiplied by δ = 31 m.

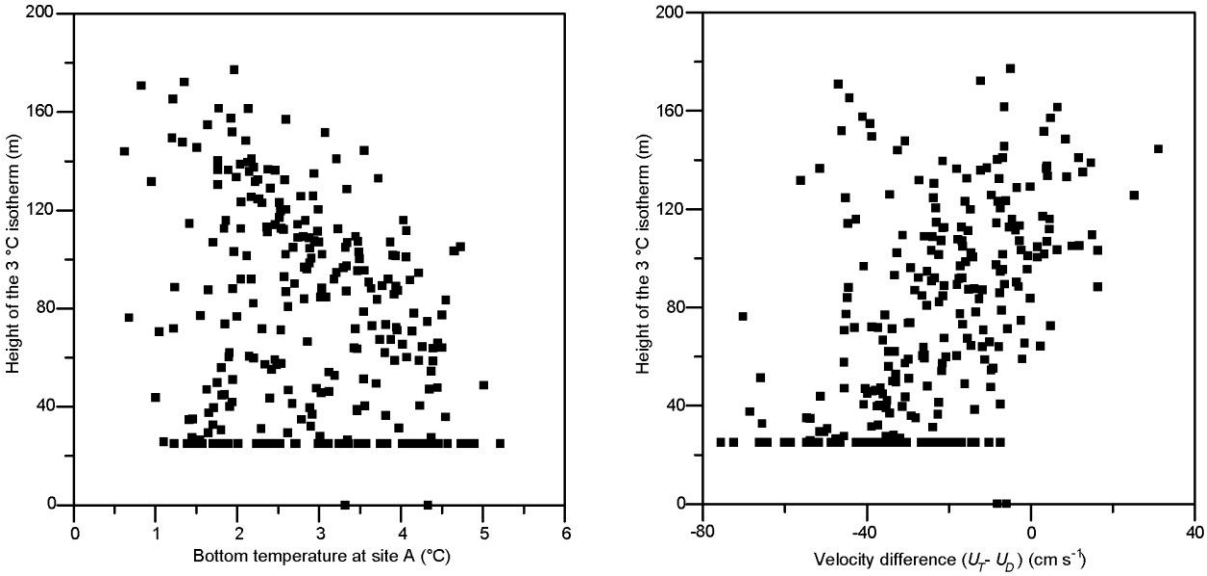

Figure S7. Daily values of estimated height of the 3 °C isotherm above bottom at site B, *z*, plotted against bottom temperature at site A **(a)** and against the velocity difference, ($U_T - U_D$), **(b)**.

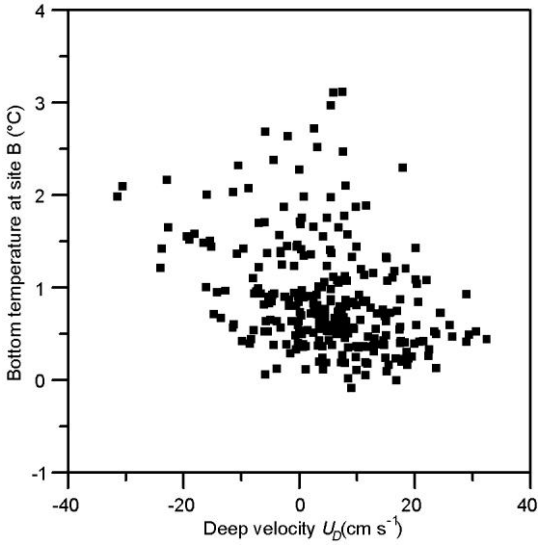

Figure S8. Daily averaged bottom temperature at site B plotted versus the deep velocity (towards 225°).

Hydraulic two-layer model

To help interpret the observed results, we consider a two-layer model with density difference $\Delta\rho$ between the two layers. The two sections in Fig. 13 in the main manuscript are illustrated in Fig. S9. On Section WV, the deep layer (the overflow layer) is assumed to flow towards the Atlantic (225°) with velocity $u_O(y)$ whereas the upper layer, the Atlantic layer, usually will flow towards the Norwegian Sea with velocity $u_A(y)$ (i.e. negative). The overflow layer is fed from the deep layer of an upstream basin that also is assumed to be two-layer and to be quiescent at all depths. This implies that the sea surface upstream (on Section East) is horizontal and so is the interface, which is assumed to be at depth d_U. On Section WV, the interface depth, $d(y)$, will, however, vary along the section (Fig. S9).

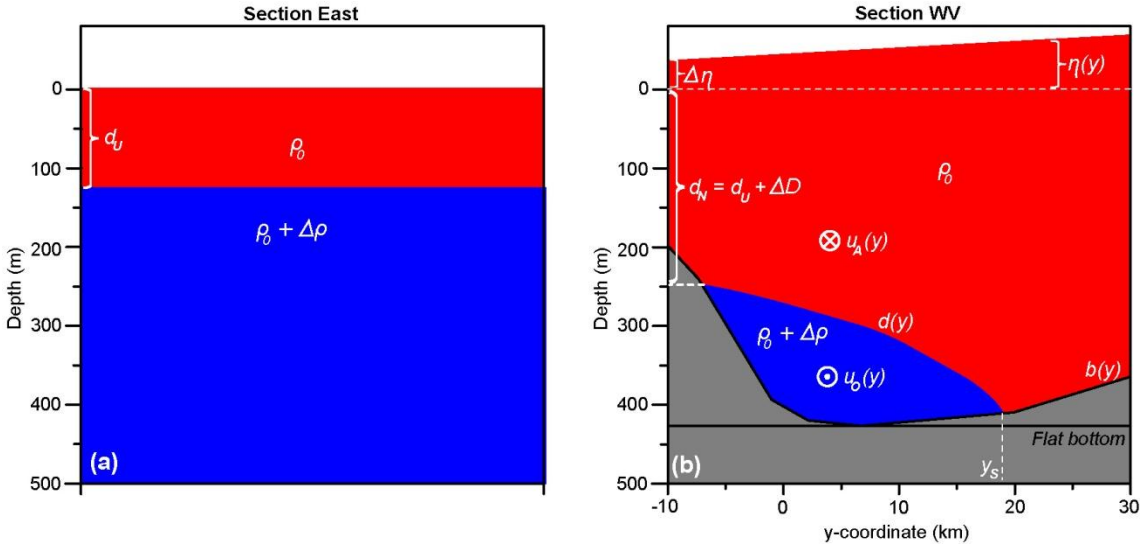

Figure S9. Schematic depiction of Section East in the upstream basin **(a)** and Section WV crossing the WV over the sill **(b)** in the two-layer model. The y-coordinate follows the y-axis on Fig. 9a in the main manuscript. The vertical axis is zero at the sea surface of the upstream basin. Velocities in the two layers on Section WV, $u_O(y)$ and $u_A(y)$, are assumed to be perpendicular to the section and are defined to be positive towards the Atlantic (out of the paper). The model is run both with real (idealized) bottom topography $b(y)$ and with a flat bottom at sill depth.

The assumption of geostrophy determines the variation of the sea surface height, $\eta(y)$, on Section WV:

$$f \cdot u_A = -g \cdot \frac{\partial \eta}{\partial y} \quad \Longrightarrow \quad \eta(y) = \Delta\eta - \frac{f}{g}\int u_A dy \qquad \text{(S1)}$$

and the variation of the interface depth:

$$f \cdot (u_A - u_O) = -g' \cdot \frac{\partial d}{\partial y} \quad \Longrightarrow \quad d(y) = d_N - \frac{f}{g'}\int (u_A - u_O) dy \qquad \text{(S2)}$$

where f is the Coriolis parameter and g and g' are the gravity and reduced gravity ($g'=g\cdot\Delta\rho/\rho_0$), respectively. $\Delta\eta$ is the sea surface height in the northwestern end of Section WV (y = -10 km) relative to the sea surface height on Section East, which is set to zero. Similarly, d_N is the interface depth in the northwestern end of Section WV.

The model is intended to represent a strong overflow similar to the one through the Faroe Bank Channel, for which the volume transport has been shown to be controlled by the along-flow

pressure difference (p_U - p_S) where p_U and p_S are the pressure at the depth of the overflow upstream and at the sill, respectively (Olsen et al., 2008). Consistent with that, we will assume frictionless flow and use the Work-Energy Theorem along a streamline in the form of the Bernoulli equation. For simplicity, we choose to follow a water parcel that does not change its depth when moving from the upstream basin to the sill (curved white arrow on Fig. 13 in the main manuscript). For this case, the Bernoulli equation has the simple form:

$$½ \cdot u_O^2(y) = \frac{1}{\rho_0} \cdot (p_U - p_S) = g' \cdot (d(y) - d_U) - g \cdot \eta(y) = g' \cdot \Delta D - g \cdot \Delta\eta + f \cdot \int u_O dy \qquad \text{(S3)}$$

where we have utilized that the pressure difference (p_U - p_S) derives partly from a change in interface depth and partly from a change in sea level. In the last term of Eq. (S3), we have inserted Eqs. (S1) and (S2). Most water parcels that join the overflow will change their depth, which means that the pressure terms may change, but this will be cancelled by the associated change in potential energy so that Eq. (S3) should be valid as long as the flow is inviscid. The volume transport of overflow water is found by horizontal integration:

$$Q_O = \int u_O(y) \cdot \big(b(y) - d(y)\big) dy \qquad \text{(S4)}$$

where *b(y)* is the bottom depth along Section WV (Fig. S9). These equations are not sufficient to give a unique solution and a definite value for the volume transport. To circumvent this ambiguity, we have added the assumption, common in hydraulic theory (Whitehead, 1998), that the appropriate solution is the one that maximizes volume transport for the specified forcing. Even if this assumption should not be valid, this guarantees that the model gives an upper value for the transport under the other assumptions made.

For the special case of a flat bottom of depth B, $\Delta\eta$ = 0, and $u_A(y)$ = 0, the equations may be solved analytically to give the traditional formula for a wide rectangular channel (Whitehead, 1998):

$$Q_O = \frac{g\prime}{2 \cdot f} \cdot (B - d_U)^2 \qquad \text{(S5)}$$

For realistic topography, equations (S1) to (S4) may be solved by integrating numerically from the Icelandic end of Section WV, except that initial values for the two arbitrary constants, $\Delta\eta$ and d_N (= d_U + ΔD) also have to be specified. The difference in sea level, $\Delta\eta$, may be considered as an external forcing factor for the overflow together with the upstream interface depth, d_U, and the velocity of the Atlantic layer over the sill, $u_A(y)$. In the numerical algorithm, the other arbitrary constant, d_N, is then varied to maximize volume transport.

To avoid any complications from flow over the shelf, the model is assumed to "begin" at the Icelandic shelf break at a bottom depth of 200 m and we envisage a vertical wall at this location, which is 10 km northwest of site B (y = -10 km). The bottom topography in the model, *b(y)*, is based on Fig. 9b in the main manuscript and has a sill depth of 425 m.

We will use the σ_θ = 27.8 kg m^{-3} isopycnal to define the interface and realistic values for the upstream interface depth, d_U, may be determined from hydrographic observations on the Icelandic Krossanes KR-4 standard station at 65°N east of Iceland. The upstream interface has an annually averaged depth ≈125 m (Olsen et al., 2016). The density in the surface layer over the WV may be quite high indicating absence of Atlantic water, but most of the time it is ≤ 27.3 kg m^{-3} (Fig. S10). East

of Iceland, near-surface densities are generally higher (Olsen et al., 2016), but they have less effect since the interface is shallower than over the WV. A realistic value for Δρ would therefore be (27.8 – 27.3) kg m^{-3} = 0.5 kg m^{-3}.

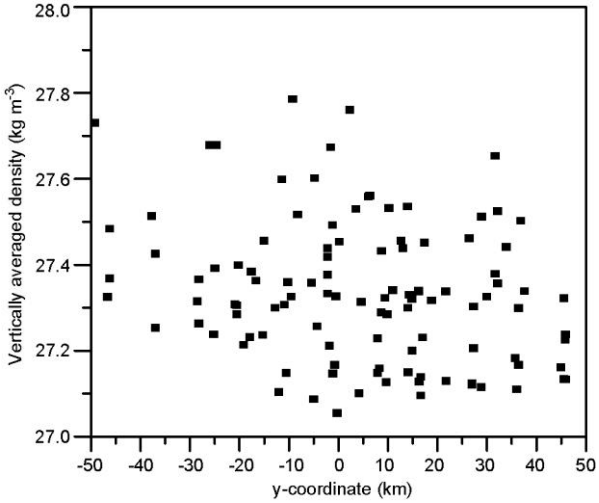

Figure S10. Density (σ_t) averaged from the surface to 100 m depth for CTD stations along the section defined in Fig. 9a in the main manuscript.

The model has been run with various combinations of the forcing parameters: $\Delta\rho$, u_A, d_U, and $\Delta\eta$ as listed in Table S2. To see the effect of topography, we also run the model with a flat bottom (Fig. S9b), which has a constant depth of 425 m from the shelf edge southeastwards. The first row in Table S2 has no Atlantic inflow (u_A = 0 and $\Delta\eta$ = 0) but realistic values for $\Delta\rho$ and d_U. It shows clearly the effect of using real topography rather than a flat bottom. For the flat bottom, the model gives the same value as would have been found by using Eq. (S5), but the real topography reduces this by almost 50%. Rows two and three in Table S2 illustrate the effects of varying $\Delta\rho$ and d_U with no Atlantic inflow (u_A = 0 and $\Delta\eta$ = 0).

Table S2. Results of model runs with a flat bottom and with realistic bottom topography. Q_O is the overflow volume transport. y_S is the southeasternmost extent of the overflow layer at least 2 m thick. W is the width of the overflow layer. u_0 is velocity at site B (y = 0). H_m is the maximum height of the overflow layer along the section. q_m is the maximum overflow transport density along the section and y_q is the location (y-coordinate) where this occurs. q_0 is the overflow transport density at site B (y = 0). u_A is assumed not to vary with y over the whole model domain.

Forcing parameters				Flat	Real bottom topography							
$\Delta\rho$	u_A	d_U	$\Delta\eta$	Q_O	Q_O	y_S	W	u_0	H_m	q_m	y_q	q_0
kg·m^{-3}	cm·s^{-1}	m	cm	Sv	Sv	km	km	cm·s^{-1}	m	m^2·s^{-1}	km	m^2·s^{-1}
0.50	0	125	0	1.64	0.89	2.1	12.1	140	115	128	-1.0	101
0.25	0	125	0	0.82	0.23	-2.4	7.6	0	82	45	-5.3	0
0.50	0	100	0	1.93	1.17	2.7	12.7	140	140	159	-1.0	136
0.50	0	125	10	0.16	0.09	3.0	6.5	53	46	23	0.5	22
0.50	-20	125	0	1.24	0.52	0.4	10.4	140	86	76	-2.8	25
0.50	-20	125	10	0.10	0.00	0.8	2.5	30	11	2	-0.3	2

The bottommost three rows in Table S2 show the effects of non-zero values for u_A and $\Delta\eta$. For simplicity, we assume in each case that u_A does not vary with y over the model domain. Both u_A and $\Delta\eta$ affect the barotropic (sea level induced) pressure difference and may reduce the volume transport considerably.

For the last row in the table, we have chosen values for $\Delta\rho$, d_U, and u_A that should be close to average. An average value for $\Delta\eta$ is difficult to estimate but the chosen value (10 cm) is consistent with Fig. 2 in the main manuscript. With this forcing, the velocity at site B is closer to observations although still too high (30 cm s^{-1}) while the volume transport is less than 0.01 Sv with realistic bottom topography. Thus, the model verifies that the observed Atlantic inflow is sufficient to suppress the volume transport of WV-overflow to the level observed even neglecting friction.

The model presented here can only be expected to apply to a strong overflow with a thick overflow layer. Otherwise, the effects of bottom friction will invalidate the assumptions of the Bernoulli equation and much lower velocities and transports will result. With no Atlantic inflow (u_A = 0 and $\Delta\eta$ = 0), the maximum height, H_m, of the overflow layer in the model (Table S2) is, however, considerably larger than the frictionally affected bottom layer of the Faroe Bank Channel overflow (Hansen and Østerhus, 2007). By analogy, the model therefore ought to be fairly realistic in that case.

From this, we conclude that if there was a strong overflow, it should have been observed by our moored instrumentation. Table S2 demonstrates that the maximum overflow transport density, q_m, usually occurs close to site B and that its value is similar to the overflow transport density at site B, q_0. The only exception is for the second row in Table S2 where the overflow layer does not extend to site B ($y_S < 0$), which is not consistent with our measurements.

Also, the width of the overflow layer, W, in the model is in every case less than 20 km and the overflow volume transport, Q_O, is less than or equal to q_0×(20 km) in all the cases where there is overflow at site B (all but the second row in Table S2). Thus, the model supports the claim in the main manuscript that the overflow transport density at site B multiplied by a fixed width of 20 km gives a maximum estimate of the overflow volume transport, even ignoring bottom friction.

References

Hansen, B. and Østerhus, S.: Faroe Bank Channel overflow 1995–2005, Prog. Oceanogr., 75, 817–856, doi:10.1016/j.pocean.2007.09.004, 2007.

Whitehead, J. A.: Topographic control of oceanic flows in deep passages and straits, Rev. Geophys., 36(3), 423-440, 1998.